ADVANCED MATERIALS
www.advmat.de

3D Printable and Reconfigurable Liquid Crystal Elastomers with Light-Induced Shape Memory via Dynamic Bond Exchange

*Emily C. Davidson, Arda Kotikian, Shucong Li, Joanna Aizenberg, and Jennifer A. Lewis**

3D printable and reconfigurable liquid crystal elastomers (LCEs) that reversibly shape-morph when cycled above and below their nematic-to-isotropic transition temperature (T_{NI}) are created, whose actuated shape can be locked-in via high-temperature UV exposure. By synthesizing LCE-based inks with light-triggerable dynamic bonds, printing can be harnessed to locally program their director alignment and UV light can be used to enable controlled network reconfiguration without requiring an imposed mechanical field. Using this integrated approach, 3D LCEs are constructed in both monolithic and heterogenous layouts that exhibit complex shape changes, and whose transformed shapes could be locked-in on demand.

Liquid crystal elastomers (LCEs) may find potential applications in deployable devices,[1,2] soft robotics,[3,4] and active systems that rely on artificial muscles.[5–8] LCEs directly couple stimuli-responsive changes of their local molecular order to a macroscopic shape change. When heated above their nematic-to-isotropic transition temperature (T_{NI}), programmed LCEs contract along the direction of their director alignment and expand in the orthogonal directions. Upon cooling below T_{NI}, this process reverses. To date, LCEs with programmed director alignment have been generated by a two-stage process of mechanically stretching and crosslinking,[9] an applied magnetic field,[5] or command surfaces for thin films (<50 µm).[10,11] Recently, bulk LCE films (>1 mm thick) with programmed alignment have been achieved via high operating temperature-direct ink writing (HOT-DIW), an extrusion-based 3D printing (3DP) technique.[12–14] Although these LCEs exhibit large, reversible contraction and high specific work, they must be continuously heated above their T_{NI} to maintain their actuated shape. The ability to create programmable 3D LCEs that lock-in to an actuated state on demand will both reduce their energy consumption and improve their versatility.

The integration of exchangeable dynamic bonds within LCEs is a promising approach to achieving locked-in states. While exchangeable bond strategies, such as transesterification, have been reported,[15–17] acid-catalyzed bond exchange exhibits an Arrhenius temperature dependence and requires heating above T_{NI} to induce significant transesterification.[18] Hence, this strategy limits the ability to precisely program and reprogram LCEs, since they must be processed in the isotropic state. It is also important to ensure that bond exchange cannot occur during normal use. New strategies are therefore needed in which the trigger for their bond exchange is orthogonal to the stimulus required for their actuation. One promising approach would be to harness light-mediated bond exchange through either direct (e.g., reversible anthracene or cinnamic acid cycloaddition)[19,20] or indirect (e.g., photoinitiator-triggered radical exchange leveraging addition-fragmentation chain transfer (AFT) agents, such as trithiocarbonates or allyl disulfides)[21–23] methods to achieve the desired reorganization of LCE networks.

Here, we demonstrate 3D printable and reconfigurable LCEs that lock-in on demand in response to optical stimuli allowing complex actuated states to be permanently maintained. Light-activated bond exchange ensures that the trigger for network reconfiguration is independent of the thermal stimuli needed to induce actuation. We integrate these exchangeable bonds into 3D LCE structures by first synthesizing a printable "reconfigurable" LCE-based ink composed of liquid crystal mesogens polymerized with an allyl dithiol chain extender (**Figure 1**a).[24] During printing, the director is aligned along the print path (Figure 1b). After crosslinking, the resulting LCE exhibits a fully reversible and programmable shape-change upon heating above and below its T_{NI}. When exposed to UV light during actuation, the stress in the dynamic LCE network drives bond exchange without requiring an externally imposed mechanical field, enabling the programmed actuated shape to be maintained even upon cooling to ambient conditions (Figure 1c,d). Importantly, the integration of dynamic bonds within these reconfigurable LCEs enables the generation of 3D architectures that are inaccessible by printing alone. By co-patterning LCEs

Dr. E. C. Davidson, A. Kotikian, Prof. J. Aizenberg, Prof. J. A. Lewis
John A. Paulson School of Engineering and Applied Sciences
Harvard University
Cambridge, MA 02138, USA
E-mail: jalewis@seas.harvard.edu
Dr. E. C. Davidson, A. Kotikian, Prof. J. Aizenberg, Prof. J. A. Lewis
Wyss Institute for Biologically Inspired Engineering
Harvard University
Cambridge, MA 02138, USA
S. Li, Prof. J. Aizenberg
Department of Chemistry and Chemical Biology
Harvard University
Cambridge, MA 02138, USA
The ORCID identification number(s) for the author(s) of this article can be found under https://doi.org/10.1002/adma.201905682.

DOI: 10.1002/adma.201905682

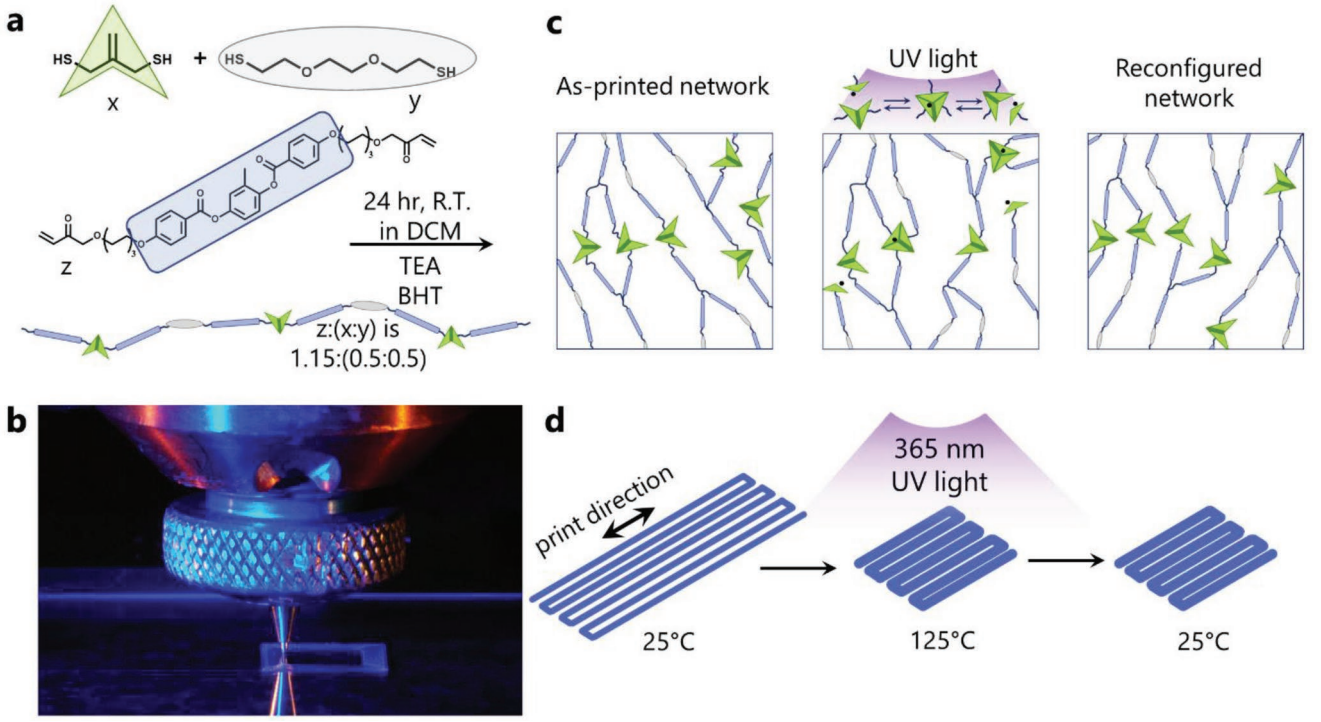

Figure 1. Reconfigurable LCE ink design and printing. a) Synthesis of the photopolymerizable LCE ink composed of exchangeable spacer (green), inert spacer (gray), and mesogen (blue). b) Image of HOT-DIW for extrusion and programming of the LCE ink with blue-light in situ photo-crosslinking. c) Schematic illustration of the LCE network reconfiguration under UV light via dynamic covalent bond exchange, and d) schematic view of LCE samples after printing (left), heating above their T_{NI} (middle), and after network reconfiguration into a locked-in state (right).

with and without dynamic bonds via multimaterial 3D printing, we demonstrate a path toward hierarchical, reconfigurable, and adaptive elastomeric architectures.

To create an LCE ink that is both printable and reconfigurable, we introduce radical-mediated dynamic covalent bonds to the network (Figure 1a). Inspired by optically reprogrammable thin films composed of a liquid crystalline network developed by McBride et al.,[25] we synthesized an LCE ink composed of a linear liquid crystalline polymer ($M_n \approx 9.8$ kDa) using an excess of a difunctional mesogen (RM82) and a 50:50 molar mixture of two dithiols (Figure 1a): allyl dithiol (ADT) (Figure S1, Supporting Information), which is well known to undergo efficient bond exchange in the presence of radicals, and ethylene dioxydiethane thiol (EDDT) (Figure 1a; Figure S2, Supporting Information). EDDT decreases the T_{NI} relative to a pure ADT ink and suppresses crystallization at room temperature (Figures S3 and S4, Supporting Information). As a control, we also synthesized an LCE ink without dynamic bonds that contains propane dithiol (PDT) rather than the dynamic ADT. Upon printing, the LCE ink with dynamic bonds is crosslinked to retain the shear-induced, programmed director alignment. However, residual photoinitiator is needed to enable subsequent bond exchange via exposure to UV light. To independently control these processes, two photoinitiators are used. Bis-acylphosphine oxide (BAPO) absorbs light at wavelengths up to 420 nm to facilitate initial crosslinking, while dimethoxyphenylacetophenone (DMPA) only absorbs light below 400 nm and is used to drive dynamic network reconfiguration.

Our LCE ink with dynamic bonds is printed at 60 °C using HOT-DIW (Figure 1b; Movie S1 and Figure S5, Supporting Information). This temperature is roughly midway between its smectic–nematic transition (T_{SmN}; 34 °C) and T_{NI} (90 °C) (Figure S3, Supporting Information). The ink exhibits the desired shear thinning behavior at 60 °C to facilitate both filamentary printing and programmed director alignment (Figure S6a, Supporting Information). This ink exhibits a liquid-like response at 60 °C (Figure S6b, Supporting Information) that quickly transitions to a solid-like response upon printing onto a glass substrate held at ambient conditions, where the ink is rapidly photo-crosslinked (λ = 400–500 nm) (Figure 1b) to form a cybotactic (or locally smectic-C) liquid crystal elastomer (Figure S4, Supporting Information). This rapid cooling and crosslinking process locks-in the alignment field obviating any effects that arise from anchoring the printed LCEs to the substrate. While the extruded ink contains multiple domains and defects, this programmed director alignment dominates its actuation behavior. Our control ink without dynamic bonds exhibits similar thermal (Figure S5, Supporting Information) and rheological properties (Figure S6, Supporting Information).

To demonstrate dynamic bond exchange-enabled locked-in states, we printed LCE strips (20 mm × 5 mm × 0.25 mm) using a 250 µm nozzle. The printed dynamic strips are optically transparent (**Figure 2**a) due to the alignment of liquid crystalline domains achieved via printing. Unbiased linear actuation of these strips occurs over a wide temperature window, beginning at 50 °C and reaching a maximum at 125 °C with a contractile

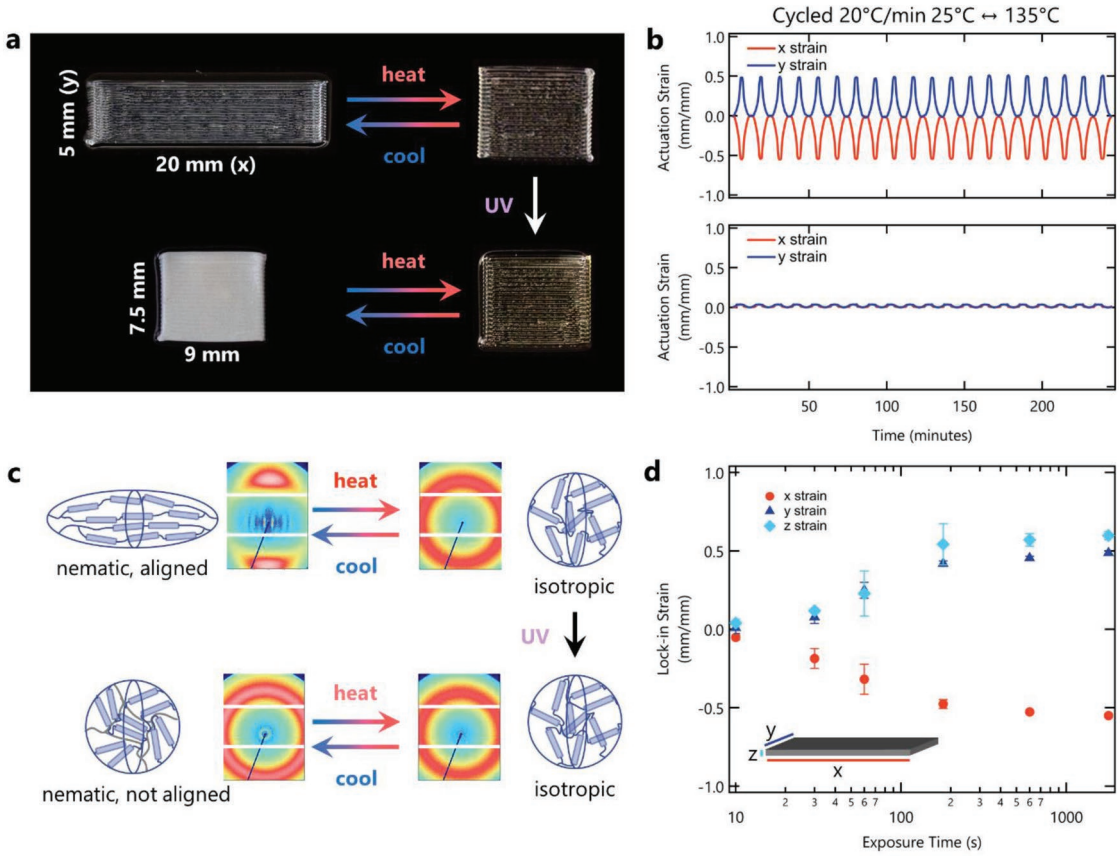

Figure 2. 3D reconfigurable LCE lock-in via UV light. a) (Top) Images of printed LCE reversibly actuating above/below the T_{NI} until (bottom) stress relaxation from UV exposure at 125 °C locks-in the actuated state. b) Strain parallel (x) and perpendicular (y) to the print path upon thermal cycling of (top) as-printed LCE and (bottom) locked-in LCE. c) Changes in mesostructure and alignment as probed via WAXS accompany both actuation and network reconfiguration. d) Degree of lock-in strain along the print path and in both perpendicular directions as a function of UV exposure time at 18 mW cm^{-2} and 125 °C. Full lock-in is achieved after ≈180 s.

strain of ≈50% along the print path (x) and an expansion of ≈50% perpendicular to the print path (y) (Figure 2; Figure S7a, Supporting Information) as well as fully reversible actuation over at least 20 cycles between 25 and 135 °C (Figure 2b, top). Control LCEs without dynamic bonds printed under optimized conditions exhibit comparable actuation behavior (Figure S7b, Supporting Information). When programmed LCE strips with dynamic bonds are exposed to UV light while actuated (Figure S8, Supporting Information), they maintain their actuated shape at ambient conditions (Figure 2a; Movie S2, Supporting Information). Upon further thermal cycling, these locked-in LCEs exhibit modest positive strains arising from thermal expansion both parallel and perpendicular to the print path, i.e., their initial molecular programming is erased (Figure 2b, bottom). Wide-angle X-ray scattering (WAXS) confirms the loss of the programmed mesogen orientation both in the isotropic state and upon cooling to ambient conditions after UV exposure (Figure 2c). Their optical properties are also impacted by the lock-in process: after high-temperature dynamic bond exchange, locked-in samples cooled to ambient conditions appear opaque (Figure 2a). This opacity arises from light scattering at the interfaces of nonaligned liquid crystalline domains.

To further explore the impact of dynamic bond exchange on LCE network reconfiguration, we characterized the mechanical and optical properties of nonaligned LCE strips (20 mm × 5 mm × 0.25 mm) both before and after high-temperature UV exposure. Over the observed stress–strain regimes of LCE mechanical response,[26] these LCE strips exhibit similar properties before and after high-temperature UV exposure. They have a comparable initial elastic response, semisoft elastic plateau stress, and final elastic modulus, emphasizing that the loss of shape recovery after UV exposure cannot be attributed to a loss of crosslink density. However, after UV exposure the semisoft elastic plateau[26] does not persist to comparably high strains (Figure S9a, Supporting Information). We attribute this change in mechanical behavior to limited local chain anisotropy from a suppressed room temperature liquid crystalline phase.[27–29] As expected, high-temperature UV-exposed samples remain optically clear to lower temperatures, showing that the T_{NI} has been suppressed (Figures S9c and S10, Supporting Information).[30,31] No significant change in properties is observed in the control LCE strips (Figure S9b,d, Supporting Information). Finally, we demonstrate that the degree of lock-in is controlled by the UV exposure time at 18 mW cm^{-2}; full lock-in is achieved after

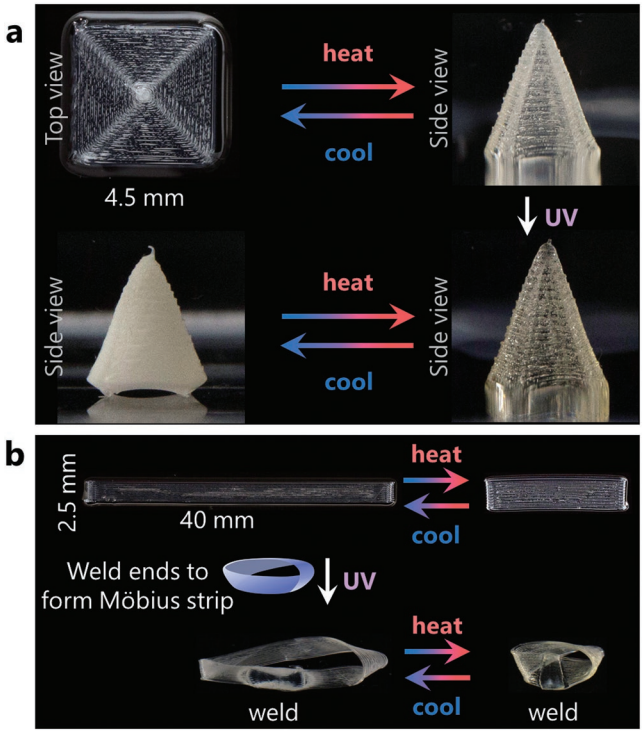

Figure 3. Reconfigurable LCEs exhibit complex shapes. a) Printed concentric squares reversibly actuate into a square cone until exposed to UV light, resulting in a locked-in, opaque cone at ambient conditions. b) A printed strip exhibits reversible linear actuation until the ends are welded together at 60 °C via dynamic bond exchange to form a reversibly actuating Möbius strip.

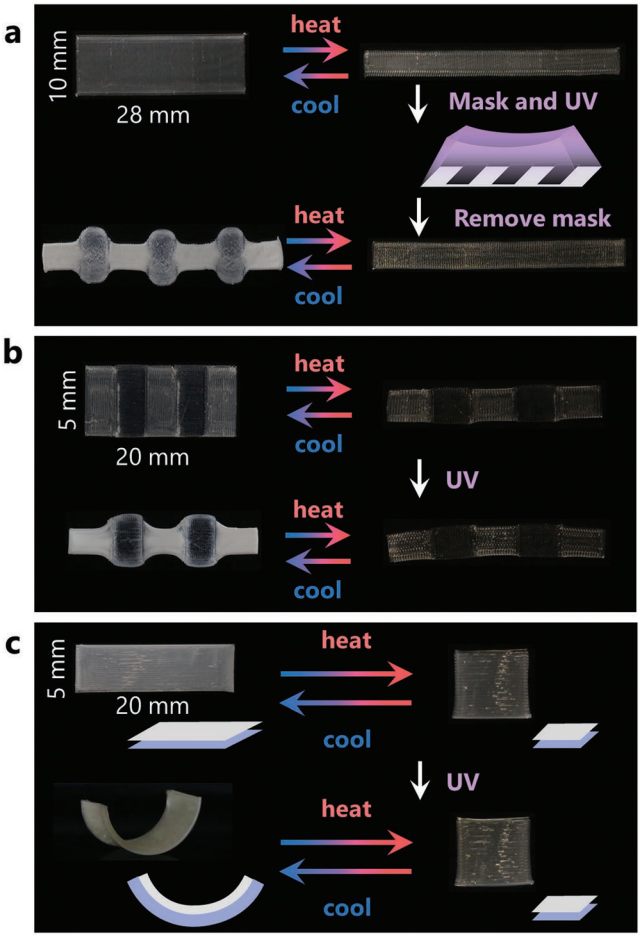

Figure 4. Patterning methods for locally reconfigured and heterogenous LCE structures. a) Locally controlled network reconfiguration via photolithography. b) Heterogenous alternating strip of LCE inks with and without dynamic bonds. c) Heterogenous printed bilayer transitions from linear actuation to bending actuation after high-temperature UV exposure.

only 180 s (Figure 2d; Figure S12c, Supporting Information). Minimal lock-in is observed in control LCE strips (i.e., without dynamic bonds) after exposure at the same intensity for 1800 s (Figure S11, Supporting Information). Confirming the coupling of molecular and macroscopic structure before and after lock-in, the degree of mesogen orientation in the programmed LCE varies smoothly with temperature for as-printed actuating strips (Figure S12a,d, Supporting Information) and lacks orientation at all temperatures in locked-in strips (Figure S12b,d, Supporting Information).

Next, we demonstrated that this approach can be extended to more complex shape morphing LCE architectures. Specifically, a square print path is used to create LCEs with dynamic bonds that reversibly transform between flat (a 0.25 mm thick film) and a conical shape (height of 7 mm). Upon exposure to UV light, the LCEs become opaque, yet retain their shape upon cooling (**Figure 3**a; Movie S3, Supporting Information). Dynamic bond exchange can also be induced in minimally actuated (60 °C) LCEs to create geometries that otherwise would be difficult to achieve.[32] However, bond exchange rates are sufficiently fast under these conditions, allowing chemical welding of programmed LCEs (Figure S13, Supporting Information) into the form of a Möbius strip that is capable of reversible actuation upon thermal cycling above and below its T_{NI} (Figure 3b) as well as reprogramming of a manually stretched printed sample so that the director is orthogonal to the original print direction (Figure S14, Supporting Information).

We can also combine printing of reconfigurable LCEs with photolithography to achieve highly localized control over their properties. As a simple demonstration, we first printed LCE strips with dynamic bonds (10 mm × 28 mm × 0.25 mm) with the director programmed along their width. Upon actuation above their T_{NI}, we placed a photomask over the printed strip that selectively blocks UV transmission in alternating masked and unmasked regions. After UV exposure and cooling, the LCE strips exhibit alternating opaque (locked-in) and clear (shape recovered) regions (**Figure 4**a). Although the combination of printing and optical patterning via photolithography is powerful, the latter method only provides planar control over the patterned regions.

As a final demonstration, we patterned LCE inks both with and without dynamic bonds via multimaterial 3D printing. Upon thermal cycling above and below their T_{NI}, these locked-in heterogeneously alternating LCE strips only transform in regions composed of LCE without dynamic bonds (Figure 4b). Heterogeneous LCE bilayers (20 mm × 5 mm × 0.50 mm) composed of both a layer with and a layer without dynamic bonds are also patterned by this method. Before UV exposure, the

bilayer exhibited a reversible contractile response, while afterward, it exhibited a bending response due to the loss of director alignment in the dynamically bonded, reconfigured layer (Figure 4c). This close coupling of network reconfiguration and programmed shape change can only be achieved in bulk shapes by 3D multimaterial printing. Despite these advances, our printable and reconfigurable LCEs do have some limitations in their present form. First, they exhibit large strains when subjected to external loads due to semisoft elasticity,[26] which prevents them from holding large weights in place in their locked-in, mechanically soft state. Second, they also lack the ability to be repeatedly switched between locked-in and normal states. Both of these capabilities are of interest for future synthetic embodiments.

In summary, we have created 3D printable and reconfigurable LCEs that reversibly shape-morph when cycled above and below their T_{NI}, whose actuated shape can be locked-in via high-temperature UV exposure. By synthesizing LCE-based inks with light-triggerable dynamic bonds, we can harness printing to locally program their director alignment and use UV light to enable controlled network reconfiguration without requiring an imposed mechanical field. Using this integrated approach, we constructed 3D LCEs in both monolithic and heterogenous layouts that exhibited complex shape changes, and whose transformed shapes could be locked-in on demand.

Experimental Section

LCE Ink Synthesis: All reagents were used without additional purification unless otherwise noted. The bond-exchangeable liquid crystalline elastomer ink was synthesized by combining the difunctional liquid crystal mesogen 1,4-bis-[4-(6-acryloyloxyhexyloxy)benzoyloxy]-2-methylbenzene (10.99 g, 1.15 equiv) (Wilshire Technologies; Princeton, NJ) with 2,2′-(ethylenedioxy)diethanethiol (1.29 g, 0.5 equiv) (Sigma-Aldrich) and allyl dithiol (0.98 g, 0.5 equiv) (synthesized) with butylated hydroxytoluene (MPI; 26.54 mg, 0.2 wt%) in dichloromethane (DCM; VWR; 33 mL) and triethylamine (TEA; 8.94 mL). The reaction was stirred for 24 h with a PTFE coated stir bar. TEA was removed by extracting the polymer in DCM twice with 1 N aqueous HCl (TCI) followed by a brine wash. DCM was dried with sodium sulfate and filtered. Photoinitiators (phenylbis(2,4,6-trimethylbenzoyl)phosphine oxide (BAPO); Sigma-Aldrich and 2,2-dimethoxy-2-phenylacetophenone (DMPA); BASF) were mixed in at 1.5 wt% each relative to the final polymer. DCM was removed by rotary evaporation followed by drying under vacuum at ambient temperature at 150 mTorr for 24 h until remaining DCM was <1 wt% by ^{1}H NMR, recovering LCE ink (9.09 g) with dynamic bonds. The control LCE ink without dynamic bonds was synthesized following the same procedure, substituting allyl dithiol with PDT (Sigma-Aldrich). Additional pure EDDT, ADT, and PDT linked LCE control inks were synthesized following the same procedure, with a mesogen:dithiol ratio of 1.15:1. Allyl dithiol was synthesized following previously reported methods and purified via distillation under vacuum.[25,33] Absolute ethanol, ethyl ether, and sulfuric acid were acquired from VWR; all other reagents for allyl dithiol synthesis were purchased from Sigma-Aldrich. ^{1}H NMR of allyl dithiol and liquid crystalline polymers was collected on a DD2 Varian 600 MHz instrument at ≈1 wt% polymer in deuterated chloroform (Cambridge Isotopes) and processed via MNova. Molecular weights were calculated based on end group analysis via NMR ($M_{n,\text{with dynamic bonds}}$ = 9770 kDa; $M_{n,\text{without dynamic bonds}}$ = 7700 kDa).

Differential Scanning Calorimetry: Approximately 10 mg samples for DSC were prepared by loading in Tzero aluminum hermetic pans. Samples were heated to 150 °C to erase thermal history, held for 5 min, cooled to −50 °C, and heated to 150 °C at a ramp rate of 10 °C min^{-1} (Q200; TA Instruments). Data shown from the second heating cycle.

Ink Rheology: Rheological properties of the LCE inks with and without dynamic bonds were characterized using a controlled stress rheometer (Discovery HR-3 Hybrid Rheometer, TA Instruments) equipped with a 20 mm steel Peltier plate geometry and a 0.250 mm gap. Prior to testing, each ink was heated above its T_{NI} to erase thermal history, and then cooled to 60 °C.

3D Printing: LCE inks were patterned using HOT-DIW. A machined copper block with RTD sensor (Omega) and two 100 W cartridge heaters (Omega) provided heating via an Omega platinum series single zone temperature controller and coupled to a Nordson 3 cc high pressure adapter. The inks were loaded into custom stainless steel 3 mL syringes fitted with 250 µm stainless steel nozzles (TecDia). The LCE ink with dynamic bonds was printed at a temperature of 60 °C and a print speed of 12 mm s^{-1}, while the LCE ink without dynamic bonds was printed at a temperature of 50 °C and a print speed of 28 mm s^{-1}. Both inks were printed at the same nozzle height of 0.125 mm, filament spacing of 0.125 mm, and an applied pressure of 385 psi using a high-pressure adapter (Nordson) controlled by a pressure box (Ultimus V, Nordson). The HOT-DIW printhead was mounted to a custom three-axis motion control stage (Aerotech Inc.). The extruded LCE ink filaments were cured in situ during printing (Omnicure S2000 with 400–500 nm filter, Excelitas) at 1 mW cm^{-2} (450 ± 80 nm sensor, SolarLight), followed by post curing for 30 min at 25 and 50 °C on each side at 3 mW cm^{-2} under inert N_2 purge. The outer edges (distance = 0.25 mm, where the nozzle makes 180° turns) of the heterogeneous LCE samples were removed to prevent edge effects from impacting the observed actuation response.

Actuation Measurements: Actuation as a function of temperature measurements was carried out by placing the printed LCE strips (20 mm × 5 mm × 0.25 mm) under a glass slide with PTFE spacers on a controlled temperature stage (Instec HCS302) that was coated with a thin layer of silicone oil. The strips were heated and cooled at 20 °C min^{-1} for cyclic measurements, while high resolution measurements of the actuation strain as a function of temperature were collected during heating at a controlled ramp rate of 4 °C min^{-1}. The strips were imaged from above (Canon T2i) and a custom MATLAB image analysis script was used to determine their dimensions for each experimental condition of interest. Using this method, the contrast of each image was first enhanced prior to conversion to greyscale. Next, the bright region was selected and fit to a rectangle. Finally, the exported x and y dimensions were converted to strains in x and y.

LCE Network Reconfiguration: Lock-in via network reconfiguration was performed by heating printed LCE samples to 125 °C in silicone oil followed by exposure to UV light (Omnicure S2000 with 320–500 nm filter) at 18 mW cm^{-2} (UVA A&B sensor, SolarLight) for controlled time under an inert N_2 purge. LCE network reconfigurability was also explored at 60 °C, below their T_{NI}. Specifically, multiple printed LCEs were pressed together between two glass slides (welding) or clamped to maintain their manually reprogrammed shape while exposing them to UV light for 30 min per side (top and bottom).

Mechanical Testing: Stress–strain tests were performed on an Instron 5566 with a 100 N load cell and pneumatic grips at 0.2 mm s^{-1}. Nonaligned LCE strips (20 mm × 5 mm × 0.25 mm) were prepared by printing samples without incident UV light and then heating them from 25 to 110 °C at 10 °C min^{-1} to erase their shear-induced director alignment prior to crosslinking. These samples were then placed on a glass plate with a thin layer of silicone oil at 125 °C under an inert N_2 purge and exposed to UV at 18 mW cm^{-2}. For adhesion tests, printed and crosslinked LCE strips (20 mm × 5 mm × 0.25 mm) were cleaned to remove any residual silicone oil by soaking in hexanes and then cut to form two 10 mm × 5 mm × 0.25 mm strips. Each strip was placed between two clamped sheets of glass held at 60 °C. Chemically adhered samples were exposed to UV at 18 mW cm^{-2} for 30 min per side (top and bottom).

Wide-Angle X-ray Scattering: X-ray measurements were performed on a SAXSLAB system with a Rigaku 002 microfocus X-ray source ($CuK_{\alpha 1}$ = 1.5409 Å) and sample to detector (PILATUS 200K, Dectris)

distance of 109.1 mm. 250 µm thick printed samples and 500 µm thick locked-in samples were exposed for 5 min (ambient conditions) or 30 s (on heating) (Linkam Scientific, HCSX350). Heated samples were reloaded at each temperature to ensure that order parameters reflected unbiased degrees of orientation. Data were reduced using the Nika macro for Igor Pro. Orientational order parameters $<P_2>$ were calculated by extracting the mesogen scattering peak intensity as a function of azimuthal angle, masking the beamstop and detector gap regions, and integrating intensity versus azimuthal angle via a custom MATLAB script.

Supporting Information

Supporting Information is available from the Wiley Online Library or from the author.

Acknowledgements

The authors gratefully acknowledge support via ARO MURI award W911NF-17-1-0351 Adaptive Self-Assembled Systems (ASSEMBLE). This work made use of shared experimental facilities at Harvard University and MIT supported in part by the MRSEC program of the National Science Foundation under awards DMR-1420570 (Harvard) and DMR-1419807 (MIT). A.K. acknowledges support from the NSF Graduate Research Fellowship program. Finally, the authors thank L.K. Sanders and C. Settens for technical assistance.

Conflict of Interest

J.A.L. is a co-founder of Voxel8, Inc., a multimaterial 3D printing company.

Keywords

3D printing, dynamic covalent bonds, light responsive, liquid crystal elastomers, shape memory

Received: September 1, 2019
Revised: October 6, 2019
Published online:

[1] H. Aharoni, Y. Xia, X. Y. Zhang, R. D. Kamien, S. Yang, *Proc. Natl. Acad. Sci. USA* **2018**, *115*, 7206.
[2] R. R. Kohlmeyer, J. Chen, *Angew. Chem., Int. Ed.* **2013**, *52*, 9234.
[3] M. Camacho-Lopez, H. Finkelmann, P. Palffy-Muhoray, M. Shelley, *Nat. Mater.* **2004**, *3*, 307.
[4] M. Rogoz, H. Zeng, C. Xuan, D. S. Wiersma, P. Wasylczyk, *Adv. Opt. Mater.* **2016**, *4*, 1689.
[5] Y. X. Yao, J. T. Waters, A. V. Shneidman, J. X. Cui, X. G. Wang, N. K. Mandsberg, S. C. Li, A. C. Balazs, J. Aizenberg, *Proc. Natl. Acad. Sci. USA* **2018**, *115*, 12950.
[6] C. L. van Oosten, C. W. M. Bastiaansen, D. J. Broer, *Nat. Mater.* **2009**, *8*, 677.
[7] C. Ohm, C. Serra, R. Zentel, *Adv. Mater.* **2009**, *21*, 4859.
[8] D. L. Thomsen, P. Keller, J. Naciri, R. Pink, H. Jeon, D. Shenoy, B. R. Ratna, *Macromolecules* **2001**, *34*, 5868.
[9] J. Kupfer, H. Finkelmann, *Makromol. Chem., Rapid Commun.* **1991**, *12*, 717.
[10] L. T. de Haan, V. Gimenez-Pinto, A. Konya, T. S. Nguyen, J. M. N. Verjans, C. Sanchez-Somolinos, J. V. Selinger, R. L. B. Selinger, D. J. Broer, A. P. H. J. Schenning, *Adv. Funct. Mater.* **2014**, *24*, 1251.
[11] T. H. Ware, M. E. McConney, J. J. Wie, V. P. Tondiglia, T. J. White, *Science* **2015**, *347*, 982.
[12] C. P. Ambulo, J. J. Burroughs, J. M. Boothby, H. Kim, M. R. Shankar, T. H. Ware, *ACS Appl. Mater. Interfaces* **2017**, *9*, 37332.
[13] M. Lopez-Valdeolivas, D. Q. Liu, D. J. Broer, C. Sanchez-Somolinos, *Macromol. Rapid Commun.* **2018**, *39*, 1700710.
[14] A. Kotikian, R. L. Truby, J. W. Boley, T. J. White, J. A. Lewis, *Adv. Mater.* **2018**, *30*, 1706164.
[15] Z. Q. Pei, Y. Yang, Q. M. Chen, E. M. Terentjev, Y. Wei, Y. Ji, *Nat. Mater.* **2014**, *13*, 36.
[16] Z. J. Wang, H. M. Tian, Q. G. He, S. Q. Cai, *ACS Appl. Mater. Interfaces* **2017**, *9*, 33119.
[17] Z. B. Wen, M. K. McBride, X. P. Zhang, X. Han, A. M. Martinez, R. F. Shao, C. H. Zhu, R. Visvanathan, N. A. Clark, Y. Z. Wang, K. K. Yang, C. N. Bowman, *Macromolecules* **2018**, *51*, 5812.
[18] D. W. Hanzon, N. A. Traugutt, M. K. McBride, C. N. Bowman, C. M. Yakacki, K. Yu, *Soft Matter* **2018**, *14*, 951.
[19] M. Gernhardt, E. Blasco, M. Hippler, J. Blinco, M. Bastmeyer, M. Wegener, H. Frisch, C. Barner-Kowollik, *Adv. Mater.* **2019**, *31*, 1901269.
[20] A. Lendlein, H. Y. Jiang, O. Junger, R. Langer, *Nature* **2005**, *434*, 879.
[21] T. F. Scott, A. D. Schneider, W. D. Cook, C. N. Bowman, *Science* **2005**, *308*, 1615.
[22] C. J. Kloxin, C. N. Bowman, *Chem. Soc. Rev.* **2013**, *42*, 7161.
[23] R. Nicolay, J. Kamada, A. Van Wassen, K. Matyjaszewski, *Macromolecules* **2010**, *43*, 4355.
[24] D. P. Nair, M. Podgorski, S. Chatani, T. Gong, W. X. Xi, C. R. Fenoli, C. N. Bowman, *Chem. Mater.* **2014**, *26*, 724.
[25] M. K. McBride, M. Hendrikx, D. Q. Liu, B. T. Worrell, D. J. Broer, C. N. Bowman, *Adv. Mater.* **2017**, *29*, 1606509.
[26] M. Warner, P. Bladon, E. M. Terentjev, *J. Phys. II* **1994**, *4*, 93.
[27] K. Urayama, E. Kohmon, M. Kojima, T. Takigawa, *Macromolecules* **2009**, *42*, 4084.
[28] N. A. Traugutt, R. H. Volpe, M. S. Bollinger, M. O. Saed, A. H. Torbati, K. Yu, N. Dadivanyan, C. M. Yakacki, *Soft Matter* **2017**, *13*, 7013.
[29] G. Skacej, C. Zannoni, *Macromolecules* **2014**, *47*, 8824.
[30] G. Skacej, *Soft Matter* **2018**, *14*, 1408.
[31] F. J. Davis, G. R. Mitchell, *Polymer* **1996**, *37*, 1345.
[32] M. K. McBride, A. M. Martinez, L. Cox, M. Alim, K. Childress, M. Beiswinger, M. Podgorski, B. T. Worrell, J. Killgore, C. N. Bowman, *Sci. Adv.* **2018**, *4*, eaat4634.
[33] R. A. Evans, E. Rizzardo, *Macromolecules* **1996**, *29*, 6983.

